Langmuir

Article

pubs.acs.org/Langmuir

Evaporation Kinetics in Swollen Porous Polymeric Networks

Emilia V. Silletta,[†] Manuel I. Velasco,[†] César G. Gómez,[‡] Rodolfo H. Acosta,*[,†] Miriam C. Strumia,[‡] and Gustavo A. Monti[†]

[†]FaMAF-Universidad Nacional de Córdoba and IFEG-CONICET, 5000 Córdoba, Argentina

[‡]Departamento de Química Orgánica, Facultad de Ciencias Químicas (IMBIV-CONICET), Universidad Nacional de Córdoba, Haya de la Torre y Medina Allende, Edificio de Ciencias II - Ciudad Universitaria, 5000 Córdoba, Argentina

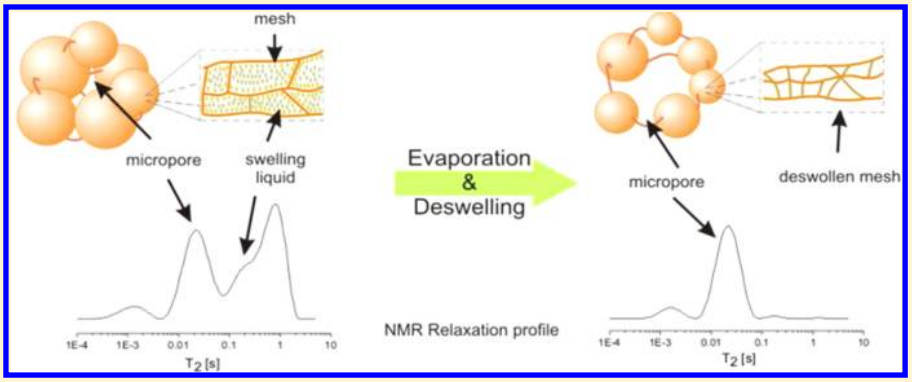

ABSTRACT: NMR is a fast, nondestructive, and noninvasive technique that can provide information about the pore structure of macroporous polymer beads and the dynamics of liquids confined in them. In this work, we describe the study of the pore structure of the macroporous polymer of ethylene glycol dimethacrylate and 2-hydroxyethyl methacrylate [poly(EGDMA-*co*-HEMA)] in the dry but also in the swollen state by measuring relaxation times of liquids contained in the polymer network. The results show that the pore architecture differs from the dry to the soaked state. The behavior of polar liquids during evaporation and deswelling dynamics is monitored and described. An internal migration of water from the swollen polymer mesh into expanding pores takes place. With this procedure it is possible to obtain information about the microscopic morphology behavior of the matrix during evaporation and deswelling. This information is of great interest with the aspect of possible and future applications for these types of materials.

1. INTRODUCTION

Macroporous polymer beads, a class of polymer beads containing a permanent well-developed porous structure,[1] have a wide range of applications[2] such as support for catalysts,[3,4] immobilization of enzymes,[5,6] HPLC columns,[7−9] adsorbents and liberation of active substances,[10] adsorbents in waste treatments,[11] among others.[12] Because of their porous structure, different solutes can diffuse through the polymeric network and, depending on the interactions between the liquid and the matrix, swelling can be present.[13] Additionally, different solutes can diffuse through the polymer network depending on its pore structure. Moreover, the cross-linking degree and the interaction between the liquid and the matrix also regulate its swelling degree. We have previously reported the synthesis of heterogeneous networks obtained with several cross-linking degrees by free-radical polymerization in suspension from 2-hydroxyethyl methacrylate (HEMA) and ethylene glycol dimethacrylate (EGDMA). It is well-known that synthesis conditions used in the suspension polymerization influence the porosity and specific surface area of the network. Because of the hydrophilic characteristic of these materials, water not only diffuses into the pore system but also swells the network, which modifies its pore structure.[14] Because structural properties may differ from the dry to the swollen state, the examination of both is necessary. Unfortunately, most classical techniques employed in the characterization of such materials are not able to provide information about the swollen state, where its structural organization may not always be directly correlated to the dry state. This is not a minor issue because most aforementioned applications involve the polymer network in a fully or partially swollen state, and in nearly every case its performance is a sensitive function of the distribution of internal pore size. Therefore, it would be of interest to implement methods that allow the study of pore architecture in the swollen network as well as the arrangement of its mesh during the swelling or deswelling process.

Nuclear magnetic resonance (NMR) relaxation is a suitable tool for studying the molecular dynamics of different liquids spatially confined in macro-, meso-, and nanopores. In transverse relaxation experiments, relaxation sources such as diffusion inside the pore, or relaxation induced by mobility restriction of the liquid near the wall, are extremely useful in the

Received: January 3, 2014
Revised: March 15, 2014

   dx.doi.org/10.1021/la500031t | *Langmuir* XXXX, XXX, XXX−XXX

determination of structural and functional properties. In particular, the use of multipulse sequences applied to protons such as Carr−Purcell−Meiboom−Gill (^{1}H-CPMG)[15,16] allows the determination of the transverse relaxation time (T_2) of the liquid molecules inside the pore. The T_2 values can be related to the size of the pore at which the molecules are confined or more specifically to the surface to volume ratio (S/V) of the pore space.[17,18] NMR relaxation is used in the study of porous media with a great variety of characteristics such as determination of pore properties in sedimentary rocks in oil industry,[19,20] drying of cement paste,[21−23] or drying of gelatins.[24] Relaxometry has also been successfully applied to obtain information on the properties of soil,[25] moisture draining,[26] or partially saturated soil in which an evaporation process is quenched to perform stationary measures of moisture content.[27] The kinetics of an evaporation process in the gel process has been modeled and measured by time-dependent measurements of the weight of a sample undergoing a drying process.[28,29] Recently the evaporation kinetics together with a deswelling process has been reported for the porous polymeric networks used in this work by means of time-dependent weight measurements.[14]

In this work we use NMR relaxometry for the study of the evaporation process in different porous polymeric systems which can undergo a swelling process and thereby induce a modification in the pore structure of the network. Characterization of the porous networks is carried out by saturating the systems with polar and nonpolar liquids to obtain information on the swollen and nonswollen (dry) states. Additionally, evaporation kinetics are monitored for both types of fluids, and the deswelling and relaxation of the microporous network structure process can be determined for samples containing a low amount of cross-linking.

2. EXPERIMENTAL SECTION

2.1. Synthesis of the Polymeric Network. Polymer beads of ethylene glycol dimethacrylate and 2-hydroxyethyl methacrylate [poly(EGDMA-*co*- HEMA)] were synthesized by suspension as described in a previous work.[30] The reactions were carried out at 85 °C in a 250 mL round-bottom flask equipped with a reflux condenser and a magnetic stirrer on a water bath for 2 h. To obtain 10 g of dry polymer, a molar ratio of 3.0:1.0:9.3:250 of HEMA (6.2 mL), EGDMA (3.2 mL), cyclohexane (17.2 mL), and water (77.0 mL) was used in the reaction at a stirring speed of 450 rpm. Different polymeric networks were obtained when a cross-linker content of 6, 10, 17, 25, or 33 mol % of EGDMA was used (Table 1). In all the cases, BPO (0.411 g, 2.44 mol %) was added as free-radical initiator, using PVP (0.777 g, 10 mg/mL of total mixture) as a suspension stabilizer. After reaction, the resulting polymer beads were fully washed with distilled water and afterward with ethanol. This procedure removes the porogenic diluent and unreacted monomers. Samples were then dried in an oven at 70 °C until constant mass was reached. The product of each reaction was calculated as the percentage of dry polymer obtained as a function of the total mass of vinyl monomers used.

Table 1. Percentage of Cross-Linker Content and Equilibrium Swelling Ratios for Water and Heptane

sample	EGDMA (%)	Q_w water	Q_w heptane
C1	6	4.5	2.9
C2	10	4.7	3.2
C3	17	5.6	3.7
C4	25	5.4	3.5
C5	33	5.4	4.0

The resulting system consists of polymer beads that contain large agglomerates of microspheres (100−200 nm).[14] Each microsphere consists in turn of smaller nuclei (10−20 nm) which are nonporous and represent the most highly cross-linked regions of the system. The nuclei are blended to some extent where the interspace between them gives rise to small cavities or micropores (5−15 nm), which are mainly responsible for the great surface to volume ratio of this type of material. The cavities between the microspheres render a second type of intermediate void named mesopores (20−50 nm). A third type of pore between 50 nm to 100 μm corresponding to meso- and macropores appears due to interconnection of microspheres. Finally, larger pores are generated when the microspheres are agglomerated into larger irregular entities in the polymer material (1 μm to 400 μm). Figure 1 shows a schematic representation of the pore architecture network with different ranges of pore size.

2.2. NMR Relaxometry Measurements. To characterize the network in dry and swollen states, the transverse relaxation time, T_2, of the liquid inside the polymeric matrix was monitored. Because polymer networks have hydrophilic characteristics, water was used as a swelling liquid to characterize the system in the swollen state. On the other hand, as a nonpolar liquid does not interact with the network, the polymer mesh is not altered, which allows information to be attained on the unperturbed pore system. Small samples of polymer beads were immersed in a vial containing distilled water at room temperature for 24 h to reach the full swelling of the network. Samples of 75 mg weight were extracted from the vial and gently placed in a 5 mm outer diameter NMR sample tube. The sample tube was previously cut to a length of 10 mm to allow a proper evaporation of the liquids. Heptane was used as a nonpolar liquid, the same amount of sample was used, and no change in the relaxation measurements was observed for a wetting time longer than 15 min.

Relaxation experiments were performed at 25 °C using a Magritek Kea2 spectrometer operating at 60 MHz for protons. A 1.4 T permanent magnet (Varian EM360) was used in all the experiments. Liquids were allowed to evaporate, and transverse proton relaxation times were measured throughout the evaporation process by using a Carr−Purcell−Meiboom−Gill (CPMG) sequence[15,16] with an echo time of 1 ms and 6000 echoes. With this echo time it can be assured that the detected signal arises only from the solvent and not from the polymer network, whose relaxation times were determined to be on the order of microseconds. All experiments were repeated at least three times for each sample, and a maximum dispersion of 3% in the processed data was obtained.

The relaxation behavior of liquids confined in porous systems is sensitive to the molecular environment; the transverse decay rate is expected to be a sum of bulk and surface relaxation rates plus a contribution due to diffusion in the presence of magnetic field gradients:

$$\frac{1}{T_2} = \frac{1}{T_{2,\mathrm{b}}} + \frac{1}{T_{2,\mathrm{s}}} + \frac{1}{T_{2,\mathrm{D}}} \tag{1}$$

Bulk relaxation times are not considered, as they were determined to be 2.5 and 2.3 s for water and heptane, respectively. At first order, the T_2 surface relaxation contribution is proportional to the local surface to volume ratio (S/V) of the pore space, where the proportionality constant ρ is the surface relaxivity. Assuming a spherical pore geometry, the diameter of the pore space d can be determined if the surface relaxivity is known.

$$\frac{1}{T_{2,\mathrm{s}}} \cong \rho\frac{S}{V} \rightarrow d = 6\rho T_{2,\mathrm{s}} \tag{2}$$

Signal attenuation due to diffusion in internal field gradients was discarded, as T_2 curves for different echoes times, ranging from 500 μs to 5 ms, were indistinguishable within the experimental error.[31]

For systems with a variable pore size, a distribution of T_2 values is expected. These distribution functions were obtained by using an inverse Laplace transform (ILT) algorithm based on the Tikhonov regularization method.[32,33]

dx.doi.org/10.1021/la500031t | Langmuir XXXX, XXX, XXX−XXX

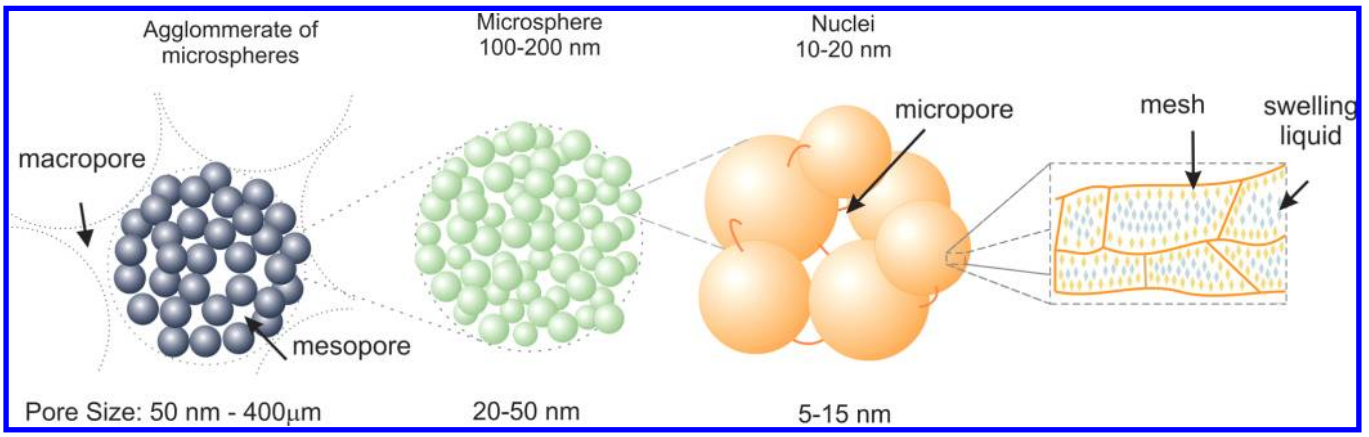

Figure 1. Distribution of pore sizes present in the network.

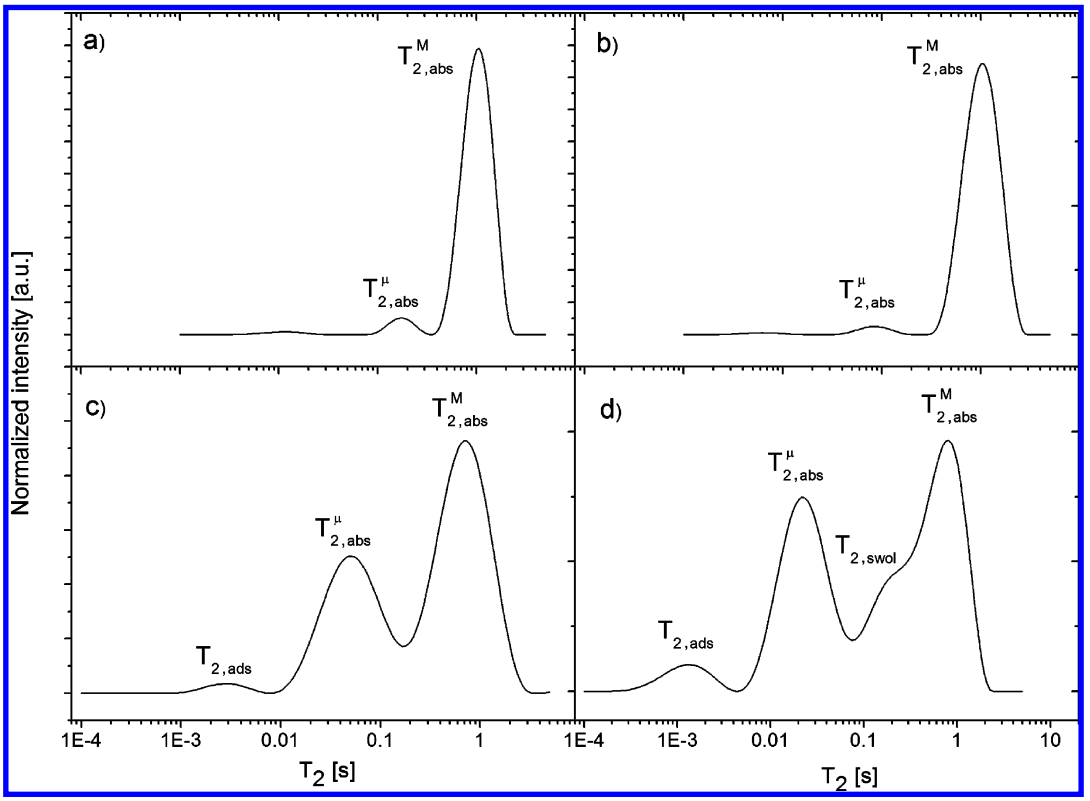

Figure 2. Relaxation distribution functions: (a) Sample C5 (33% EGDMA) saturated with heptane; (b) C1 (6% EGDMA); (c) sample C5 saturated with water; (d) sample C1 saturated with water. The effect of swelling can be observed by the appearance of the relaxation distribution $T_{2,swol}$ for protons corresponding to water in panel d.

3. RESULTS AND DISCUSSION

3.1. Relaxation Dependence on Network Morphology. The T_2 relaxation time distribution of heptane and water in saturated samples C5 and C1 is shown in Figure 2. Relaxation time distributions for liquid absorbed in the macro- and mesopores are denoted as $T^M_{2,abs}$, while lower relaxation time values are assigned to the liquid absorbed in the micropores ($T^\mu_{2,abs}$) or adsorbed in the network mesh ($T_{2,ads}$). Because heptane shows little tendency to reside at or near the polymer polar surface, the interaction with the matrix is weak; therefore, it does not swell the polymer and the solvent molecules are mainly located in the macropores. A minor population is placed in the mesopores, revealing that in the dry state the main contribution to the porosity of the polymer is given by the larger pore spaces. Additionally, the relaxation times for heptane are, in general, longer than those observed for water due to the weak interaction of nonpolar liquids with the polymer mesh.

When the networks are fully saturated in water, the relaxation time distribution profiles change significantly. Figure 2c shows the data corresponding to sample C5, with 33% EGDMA content, which has been shown to render a very stable network with a small degree of swelling and minor changes in the pore size distribution with respect to the dry state.[14] In addition to the relaxation times corresponding to liquid absorbed in the meso- and macropores, a small distribution with short relaxation times is present, which can be assigned to adsorbed water in the polymer mesh ($T_{2,ads}$). As the cross-linker content is reduced, the network is more capable of undergoing swelling,

dx.doi.org/10.1021/la500031t | Langmuir XXXX, XXX, XXX–XXX

and the water contained within the swollen mesh behaves as a new pore space with relaxation time distribution $T_{2,swol}$. The great amounts of water that network C1 (6% of EGDMA) can uptake render a $T_{2,swol}$ distribution with values higher than water absorbed in the micropores (Figure 2d). To validate this assumption, it is necessary to inspect previous results on determination of water uptake.

The amount of liquid that the network can uptake depends on its affinity for the polymer chains, the cross-linking density of the network, and its pore architecture. In the case of water, it can be either absorbed (w_{abs}) into the pore system or adsorbed (w_{ads}) by the network mesh (Figure 1). A measure of the liquid content in a saturated sample is the equilibrium weight swelling ratio, Q_w^{bulk}, which can be attained from the total mass of swollen sample (w_{swol}) and the dry polymer mass (w_{dry}) as follows:

$$Q_w^{bulk} = \frac{w_{swol}}{w_{dry}} = \frac{w_{abs} + w_{ads} + w_{dry}}{w_{dry}}.$$

Calculated Q_w^{bulk} values for water and heptane are summarized in Table 1. It is possible to observe that water swells the network mesh and can also be absorbed in the macro-, meso-, and micropores. Contrarily, heptane shows poor tendency to reside near polar surfaces of the polymer matrix; therefore, the heptane uptake amount in the network will be smaller than that found for water. However, there is a similar trend as a function of the cross-linker content. The equation that describes the variation of the pore volume from the dry state upon swelling was recently derived:[14]

$$\Delta v^{pore} = \frac{(Q_w^{bulk} - Q_w^{ske})}{\delta^{water}\left(\frac{1}{\delta_{dry}^{bulk}} - \delta_{dry}^{ske}\right)} - 1 \quad (3)$$

where $Q_w^{ske} = (w_{ads} + w_{dry})/ w_{dry})$ is the equilibrium swelling weight ratio for the skeletal polymeric chains, δ^{water} is the density of water, δ_{dry}^{bulk} is the density of a dry bulk network, and δ_{dry}^{ske} is the skeletal density of a dry sample. The volume of water adsorbed by the network can be calculated as $v_{ads}^{water} = (Q_w^{ske} - 1)/\delta^{water}$. In a previous work, Q_w^{ske} was obtained by measuring the weight of a sample during a water evaporation process.[14] The percentage of water adsorbed by the network obtained in ref 14 is plotted together (Figure 3) with the areas under the relaxation time distributions corresponding to $T_{2,ads}$ plus $T_{2,swol}$. The remarkable coincidence indicates that the assignment of T_2 distribution to the swollen water is correct. It is worth to note that $T_{2,swol}$ can only be distinguished for water saturated samples C1 and C2, where the low percentage of cross-linker renders a soft network that is capable of swelling.

The ability of the system to swell leads to a change in the size distribution of the polymer beads, which affects the overall pore space. A maximum variation of pore volume of 30% was observed for a 17% EGDMA content.[14] A high concentration of EGDMA leads to an increase in the number of pendant vinyl groups, giving rise to an earlier phase separation in the preparation process.[1] In these systems, nuclei are more rigid and present a higher aggregation of small microspheres, resulting in a network with a lower average pore size and more stable pore system.[1,6,14] An interesting property of sample C1, previously reported, is that the pore volume can actually decrease upon expansion of the polymer beads due to swelling. This effect is related to a considerable degree of expansion of

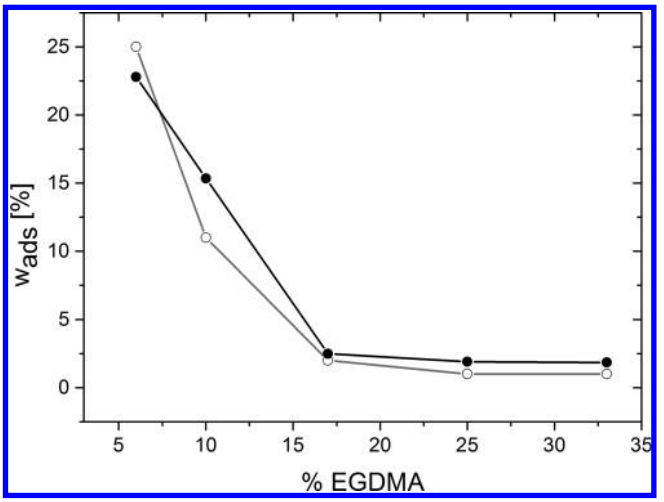

Figure 3. Percentage of adsorbed water. NMR data (filled circles) are constructed by adding the contribution of $T_{2,swol}$ and $T_{2,ads}$. Water adsorption was determined by weighting methods (open circles) as described in ref 14.

the primary particle. In this case, the primary particle undergoes deformations, giving rise to smaller overall pore volume. The same behavior is obtained in the present work for the dependence of the relaxation times on EGDMA content (Figure 4), particularly in the relaxation times of water

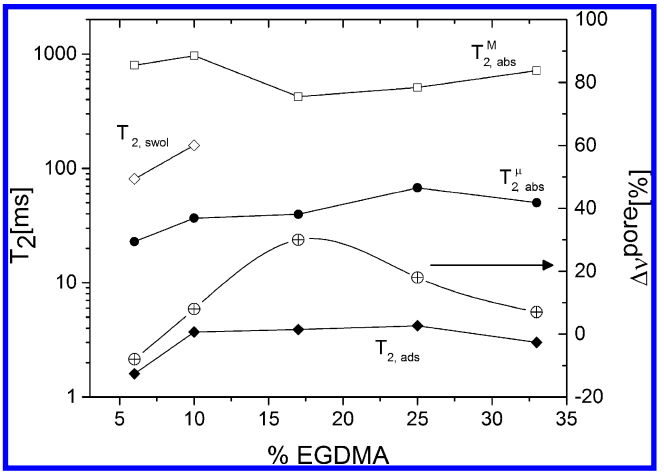

Figure 4. Mean relaxation times of the distributions obtained for water in different networks as a function of the cross-linker content. Variation of the pore volume determined by weighting methods (crossed circles) as described in ref 14.

absorbed within the micropores ($T^{\mu}_{2,abs}$) and water adsorbed in the polymer mesh, $T_{2,ads}$, where mean T_2 values for these distributions decrease with decreasing EGDMA content, indicating a smaller pore volume, in accordance with previous results (see Figure 3).[14]

3.2. Evaporation Kinetics of Nonpolar Liquids. Further information from the liquid−liquid interactions of the molecules confined in the networks can be obtained by monitoring the evaporation process. Fully saturated samples were evaporated at ambient pressure and temperature conditions. Relaxation decay curves were systematically acquired during the evaporation process. Data from the evaporation process, obtained by monitoring the evolution of the NMR signal intensity as a function of time, are in complete

dx.doi.org/10.1021/la500031t | Langmuir XXXX, XXX, XXX−XXX

agreement with data obtained by weighting the sample as a function of the total water evaporation. In this work, a complete T_2 decay was acquired every 20 min. The overall signal amplitude and T_2 contributions for different pore sizes are displayed in Figure 5 for network C5 saturated with heptane, as

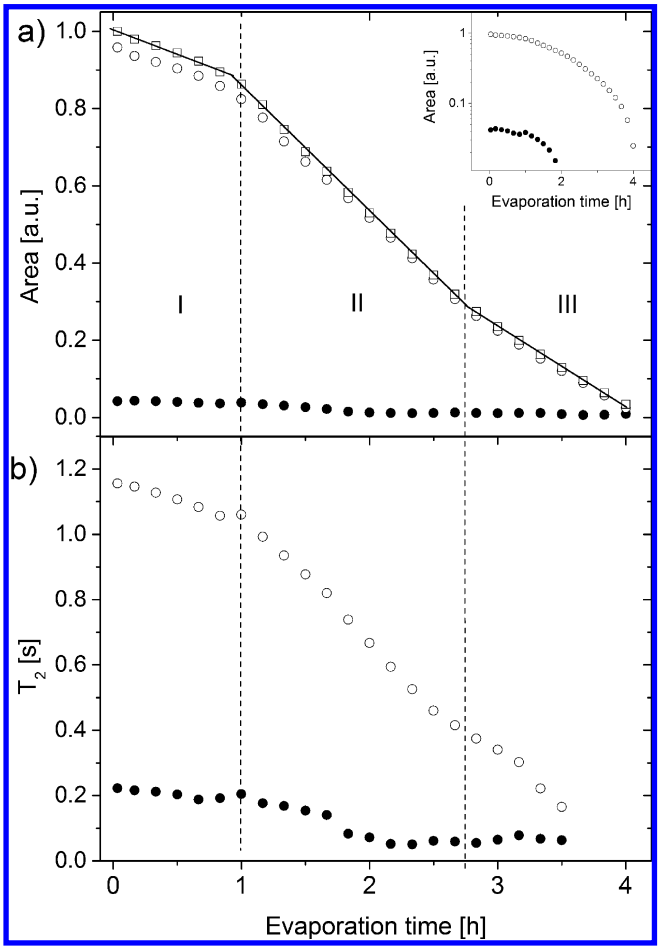

Figure 5. Evaporation kinetics of heptane in sample C5. (a) Normalized signal intensity (squares) and individual contributions from heptane in meso- and macropores (open circles) and in micropores (filled circles). (b) Mean relaxation times of the individual distributions. Three linear regimes are observed: initially for I an excess of heptane is present, II corresponds to evaporation from the whole sample, and III is the period where the micropores are fully depleted. The inset shows that the evaporation kinetics is the same for all the pore sizes.

a function of the evaporation time. Three linear decay stages (I, II, and III) with different evaporation rates are observed. Constant rate (CR) drying is expected for evaporation processes in porous materials where liquid–liquid interactions govern the kinetics. Further evaporation regimes such as first decreasing rate (FDR) that occur at longer evaporation times were not observed for these sytems.[34,35] In the linear regime, the evaporation rate is proportional to rA, where r is the specific rate of evaporation, which is expressed in grams of liquid per unit area per unit time, and A is the area of the liquid/gas interface.[28]

Stage I is the evaporation of the excess of heptane on top of the sample; as the area on top of the sample is smaller than that defined by the porous system, the relaxation rate is low. During stages II and III, the evaporation rate changes. Because the evaporation rate solely depends on the liquid, the variation in the evaporation rate can be attributed to a combination of the contributions from liquid contained in pores of different sizes to the total evaporation rate. With the experimental technique used in the present work, the contribution to the evaporation rate from different pore sizes can be distinguished. This is a remarkable difference from other experimental procedures. For each evaporation time, it is possible to deconvolute the relaxation time distribution, obtaining the contribution from each relaxation distribution to the overall signal; thus, the variation in the amount of liquid in each environment can be determined throughout the evaporation process.[27,36]

The logarithm of the area of the relaxation distributions for heptane as a function of time are shown in the inset of Figure 5. Here it can be observed that the evaporation kinetics for the different environments is the same during the whole time span. For region II, the superposition of the linear regimes due to meso- and macropore environments renders an apparently faster evaporation rate, while in stage III it is clear that the contribution to the signal is completely due to the liquid contained in the mesopores. The observation that a small amount of heptane is contained in smaller pores is due to the fact that the polarity of the network, which is mainly given by the presence of the OH groups of the HEMA, does not favor interactions between the solvent and the polymer molecules. In this situation, only superficial mesopores would be filled by heptane and the evaporation process is then the same for the whole system. The same behavior was observed for all the samples, but no correlation with the amount of cross-linker and the evaporation rates was found.

We now analyze the behavior of the mean value of the relaxation time distributions as the evaporation process takes place (Figure 5, lower panel). As previously mentioned, the relaxation times for well-defined macro- and mesopore distributions cannot be discriminated for heptane. The same applies to the small layer of excess liquid. As this layer starts to evaporate, the larger mean relaxation value shifts toward lower $T^{M}_{2,abs}$ values. In the transition from stage I to stage II, the relaxation time decay becomes more pronounced and $T^{\mu}_{2,abs}$ also starts to shift, indicating that heptane contained in the micropores is evaporating simultaneously. As heptane is evaporated, the pores become partially filled and the effective pore spaces where the liquid can diffuse become smaller which, according to eq 2, results in shorter T_2 values. It must be kept in mind that as the evaporation process takes place, the NMR signal is increasingly smaller, making the numerical algorithm used for deconvolution subject to larger uncertainties.[37]

3.3. Evaporation Kinetics of Polar Liquids. When the systems are saturated with polar liquids, water in the present case, the whole space defined by the sample topology is occupied and, additionally, swelling of the polymer matrix is produced. The evaporation dynamics present extremely different behaviors in comparison to nonpolar liquids. For networks with EGDMA content above 17 mol %, molecules in the different domains evaporate inversely to the force of association with their respective molecular environment:[28] first the molecules in the wetting liquid that surrounds the bead particles, next the macro- and mesopore molecules, and finally the molecules immobilized by adsorption to the mesh of the polymer. Liquid evaporation from the mesh does not take place at room temperature; thus, the area of distribution $T_{2,ads}$ remains constant. Figure 6 shows these behaviors for sample C5. The excess water evaporates after approximately 5 h.

dx.doi.org/10.1021/la500031t | Langmuir XXXX, XXX, XXX–XXX

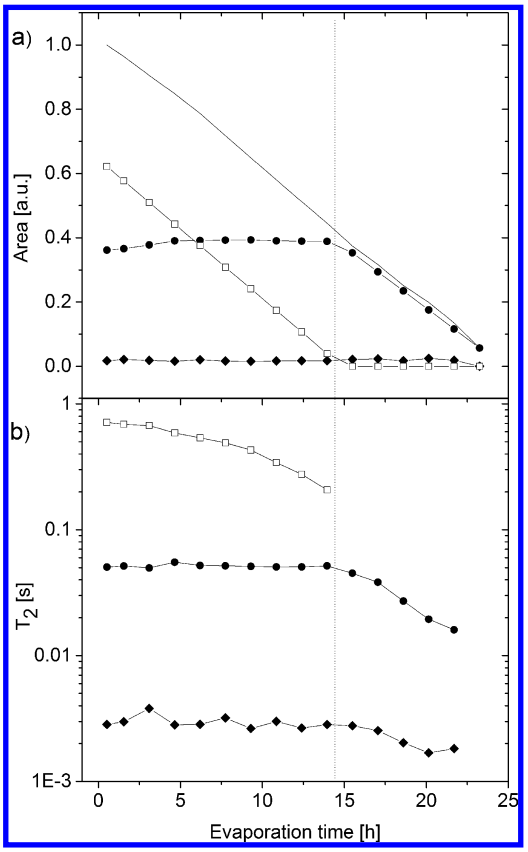

Figure 6. Evaporation of water in sample C5 discriminated by the different pores sizes through ILT from individual relaxation decays acquired during evaporation. (a) Area under each relaxation distribution time for water contained in the macropores (squares), mesopores (dots), and micropores (diamonds). The full line is the addition of all contributions. (b) Mean relaxation time value of each distribution.

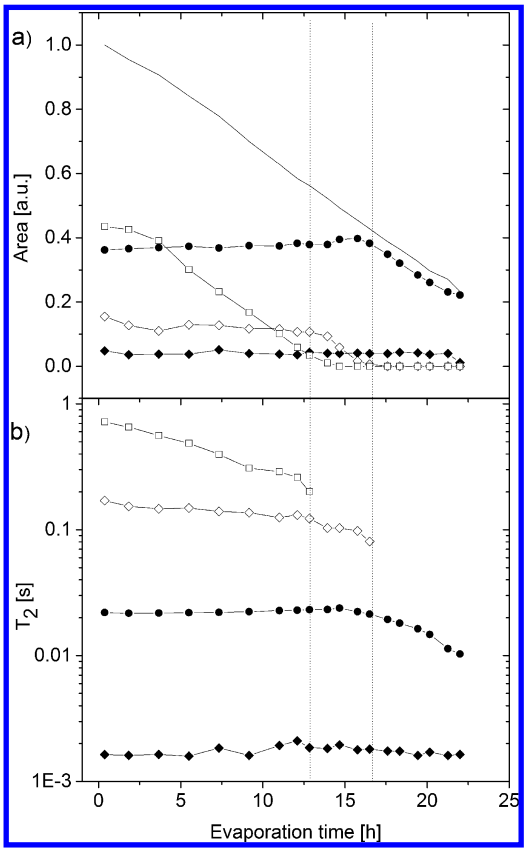

Figure 7. Evaporation of water in sample C1 discriminated by the different pores sizes through ILT from individual relaxation decays acquired during evaporation. (a) Area under each relaxation distribution time for water contained in the macropores (squares), mesopores (dots), micropores (full diamonds), and swollen mesh (open diamonds). The full line is the addition of all contributions. (b) Mean relaxation time value of each distribution.

Afterward a linear evaporation rate is observed for water corresponding to the area of distribution $T^{M}_{2,abs}$, while the rest of the areas and relaxation times remain constant. After 12.8 h, the macro- and mesopores are completely dry and evaporation of water absorbed in the micropores takes place. For networks with EGDMA content below 17 mol %, swelling of the polymer mesh is present and the evaporation dynamics are different as shown in Figure 7 for network C1. In this case, molecules corresponding to $T^{M}_{2,abs}$ evaporate completely and immediately afterward (ca. 13 h) the mesh deswelling is obvious. From Figure 7b it can be observed that the mean relaxation time for $T_{2,swol}$ is monotonically decreasing during the whole process, indicating that deswelling is always present through the evaporation of water absorbed in the meso- and macropores. However, from the areas it is clear that the deswelling process accelerates its rate immediately after the larger pores are free of water.

The most interesting behavior is that of water absorbed in the micropores. From the areas of the distribution functions it can be observed that the amount of water in these cavities remains mainly constant until the larger cavities are empty. Afterward a slight increase in the amount of absorbed molecules is observed; this water is migrating from the swollen polymer mesh into the micropores. Errede et al.[28] found that expandable networks show large empty space inside their mesh which hosts a large amount of fluid, so the earlier evaporation of molecules with liquid−liquid interaction contributes greatly to the overall evaporation kinetics. The relaxation times for water in the swollen mesh and in the micropores ($T_{2,swol}$ and $T^{\mu}_{2,abs}$) are plotted in Figure 8, where the monotonic decay of $T_{2,swol}$ indicates the shrinking of the swollen cavities, while a monotonic increase in $T^{\mu}_{2,abs}$ reveals that the micropore size is increasing until a simultaneous evaporation of water in the micropores and deswelling takes place. The evaporation of water in the micropores continues further in a situation in which swollen water is not present or is at least undetectable. This behavior is in agreement with the specific pore volume reduction upon swelling described previously.

4. CONCLUSIONS

Applications of CPMG pulse sequence for determination of pore structure in sedimentary rocks is, nowadays, a standard technique. However, to our knowledge, pore structure determination and evaporation kinetics studies on organic or macromolecular materials using CPMG and inverse Laplace transform have not yet been reported. This experiment provides information about the evaporation kinetics of liquids in a polymeric network. We have shown that with this method not only can individual evaporation processes for different pore size distributions be determined but also internal migration of water from a swollen polymer mesh into expanding pores can be measured. Moreover, this type of experiment can be carried

dx.doi.org/10.1021/la500031t | Langmuir XXXX, XXX, XXX−XXX

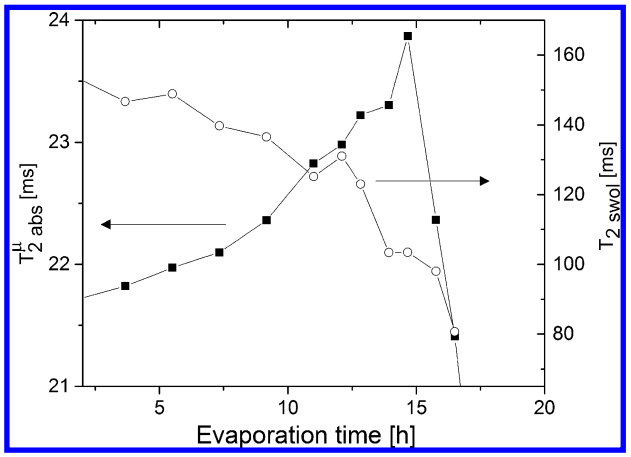

Figure 8. Relaxation times for water in the swollen mesh and in the micropores ($T_{2,swol}$ and $T^{\mu}_{2,abs}$). A section of the data from Figure 7illustrates that as the contribution from water to the swollen network diminishes the relaxation time, or pore size, water molecules in the micropores have higher relaxation times, indicating a larger pore size. Evaporation of water in the micropores starts after approximately 15 h.

out in compact benchtop NMR systems, which present a negligible stray field and can be used in reduced laboratory spaces without the safety conditions normally required for high field superconducting magnets. We envision that this easily applied technique will provide useful information not only on the morphology of organic porous polymeric systems but also on functionality in a wide range of applications.

AUTHOR INFORMATION

Corresponding Author

*E-mail: racosta@famaf.unc.edu.ar (R.H.A.).

Notes

The authors declare no competing financial interest.

ACKNOWLEDGMENTS

We thank Dr. Sophie Godefroy, Dr. Brett Ryland, and Dr. Petrik Galvosas from Victoria University of Wellington, New Zealand, for providing us with the 2D inverse Laplace transformation tool. We appreciate the financial support from CONICET, SeCyT Universidad Nacional de Córdoba, and ANPCYT PICT 2010-1096. M. I. Velasco and E. V. Silletta thank CONICET for a postdoctoral and doctoral fellowship, respectively.

REFERENCES

(1) Okay, O. Macroporous copolymer networks. *Prog. Polym. Sci.* **2000**, *25* (6), 711−779.

(2) Svec, F.; Fréchet, J. M. J. New designs of macroporous polymers and supports: From separation to biocatalysis. *Science* **1996**, *273* (5272), 205−211.

(3) Islam, S. M.; Tuhina, K.; Mubarak, M.; Mondal, P. Hydrogenation of various organic substrates using polystyrene anchored orthometallated ruthenium (II) complex as catalyst. *J. Mol. Catal. A: Chem.* **2009**, *297* (1−2), 18−25.

(4) Abu-Elfotoh, A. M.; Tsuzuki, K.; Nguyen, T. B.; Chanthamath, S.; Shibatomi, K.; Iwasa, S. Quinones synthesis via hydrogen peroxide oxidation of dihydroxy arenes catalyzed by homogeneous and macroporous-polymer-supported ruthenium catalysts. *Tetrahedron* **2013**, *69* (40), 8612−8617.

(5) Dhake, K. P.; Bhatte, K. D.; Wagh, Y. S.; Singhal, R. S.; Bhanage, B. M. Immobilization of steapsin lipase on macroporous immobead-350 for biodiesel production in solvent free system. *Biotechnol. Bioprocess Eng.* **2012**, *17* (5), 959−965.

(6) Gomez, C. G.; Strumia, M. C. Study of amino ligands fixation to macroporous supports and their influence on albumin adsorption. *J. Polym. Sci., Part A-1: Polym. Chem.* **2009**, *47* (24), 6771−6782.

(7) Gölgelioğlu, Ç.; Bayraktar, A.; Çelebi, B.; Uğuzdoğan, E.; Tuncel, A. Aqueous size exclusion chromatography in semimicro and microcolumns by newly synthesized monodisperse macroporous hydrophilic beads as a stationary phase. *J. Chromatogr., A* **2012**, *1224*, 43−50.

(8) Plieva, F. M.; Galaev, I. Y.; Mattiasson, B. Macroporous gels prepared at subzero temperatures as novel materials for chromatography of particulate-containing fluids and cell culture applications. *J. Sep. Sci.* **2007**, *30* (11), 1657−71.

(9) Lin, L. Q.; Zhang, J.; Fu, Q.; He, L. C.; Li, Y. C. Concentration and extraction of sinomenine from herb and plasma using a molecularly imprinted polymer as the stationary phase. *Anal. Chim. Acta* **2006**, *561* (1−2), 178−182.

(10) Shaha, V.; Jain, H.; Krishna, J.; Patel, P. Microsponge drug delivery: A review. *Int. J. Res. Pharm. Sci.* **2010**, *1* (2), 212−218.

(11) Tripathi, A.; Melo, J. S.; D'Souza, S. F. Uranium (VI) recovery from aqueous medium using novel floating macroporous alginate-agarose-magnetite cryobeads. *J. Hazard. Mater.* **2013**, *246−247*, 87−95.

(12) Jiang, K.; Sposito, A.; Liu, J.; Raghavan, S. R.; Devoe, D. L. Microfluidic synthesis of macroporous polymer immunobeads. *Polymer* **2012**, *53* (24), 5469−5475.

(13) Scheler, S. A novel approach to the interpretation and prediction of solvent effects in the synthesis of macroporous polymers. *J. Appl. Polym. Sci.* **2007**, *105* (5), 3121−3131.

(14) Gomez, C. G.; Pastrana, G.; Serrano, D.; Zuzek, E.; Villar, M. A.; Strumia, M. C. Macroporous poly(EGDMA-co-HEMA) networks: Morphological characterization from their behaviour in the swelling process. *Polymer* **2012**, *53* (14), 2949−2955.

(15) Carr, H. Y.; Purcell, E. M. Effects of diffusion on free precession in nuclear magnetic resonance experiments. *Phys. Rev.* **1954**, *94* (3), 630−638.

(16) Meiboom, S.; Gill, D. Modified spin-echo method for measuring nuclear relaxation times. *Rev. Sci. Instrum.* **1958**, *29* (8), 688−691.

(17) Zimmerman, J. R.; Brittin, W. E. Nuclear magnetic resonance studies in multiple phase systems: Lifetime of a water molecule in an adsorbing phase on silica gel. *J. Phys. Chem.* **1957**, *61* (10), 1328−1333.

(18) Cohen, M. H.; Mendelson, K. S. Nuclear magnetic relaxation and the internal geometry of sedimentary rocks. *J. Appl. Phys.* **1982**, *53* (2), 1127−1135.

(19) Song, Y. Q. Magnetic resonance of porous media (MRPM): A perspective. *J. Magn. Reson.* **2013**, *229*, 12−24.

(20) Kleinberg, R. L.; Kenyon, W. E.; Mitra, P. P. Mechanism of NMR Relaxation of Fluids in Rock. *J. Magn. Reson., Ser. A* **1994**, *108* (2), 206−214.

(21) Jehng, J. Y.; Sprague, D. T.; Halperin, W. P. Pore structure of hydrating cement paste by magnetic resonance relaxation analysis and freezing. *Magn. Reson. Imaging* **1996**, *14* (7−8), 785−791.

(22) McDonald, P. J.; Korb, J. P.; Mitchell, J.; Monteilhet, L. Surface relaxation and chemical exchange in hydrating cement pastes: A two-dimensional NMR relaxation study. *Phys. Rev. E* **2005**, *72* (1).

(23) Van Landeghem, M.; d'Espinose de Lacaillerie, J.-B.; Blümich, B.; Korb, J.-P.; Bresson, B. The roles of hydration and evaporation during the drying of a cement paste by localized NMR. *Cem. Concr. Res.* **2013**, *48*, 86−96.

(24) Ghoshal, S.; Mattea, C.; Stapf, S. Inhomogeneity in the drying process of gelatin film formation: NMR microscopy and relaxation study. *Chem. Phys. Lett.* **2010**, *485* (4−6), 343−347.

(25) Kleinberg, R. L. Utility of NMR T2 distributions, connection with capillary pressure, clay effect, and determination of the surface relaxivity parameter $\rho 2$. *Magn. Reson. Imaging* **1996**, *14* (7−8), 761−767.

(26) Perlo, J.; Danieli, E.; Blumich, B.; Casanova, F. Optimized slim-line logging NMR tool to measure soil moisture in situ. *J. Magn. Reson.* **2013**, *233*, 74−9.
(27) Stingaciu, L. R.; Pohlmeier, A.; Blümler, P.; Weihermüller, L.; van Dusschoten, D.; Stapf, S.; Vereecken, H. Characterization of unsaturated porous media by high-field and low-field NMR relaxometry. *Water Resour. Res.* **2009**, *45* (8), DOI: 10.1029/2008WR007459.
(28) Errede, L. A.; Kueker, M. J.; Tiers, G. V. D.; Van Bogart, J. W. C. Polymer drying, 1. Time-studies of desorption from liquid saturated poly(styrene-co-divinylbenzene) microparticles. *J. Polym. Sci., Part A-1: Polym. Chem.* **1988**, *26* (12), 3375−3389.
(29) Shahraeeni, E.; Or, D. Pore-scale analysis of evaporation and condensation dynamics in porous media. *Langmuir* **2010**, *26* (17), 13924−36.
(30) Gomez, C. G.; Alvarez Igarzabal, C. I.; Strumia, M. C. Effect of the crosslinking agent on porous networks formation of hema-based copolymers. *Polymer* **2004**, *45* (18), 6189−6194.
(31) Mitchell, J.; Chandrasekera, T. C.; Gladden, L. F. Obtaining true transverse relaxation time distributions in high-field NMR measurements of saturated porous media: Removing the influence of internal gradients. *J. Chem. Phys.* **2010**, *132* (24), 244705.
(32) Provencher, S. W. A constrained regularization method for inverting data represented by linear algebraic or integral equations. *Comput. Phys. Commun.* **1982**, *27* (3), 213−227.
(33) Tikhonov, A. N.; Arsenin, V. Y. *Solutions of ill posed problems*; Wiley: New York, 1977.
(34) Coussot, P. Scaling approach of the convective drying of a porous medium. *Eur. Phys. J. B* **2000**, *15* (3), 557−566.
(35) Chauvet, F.; Duru, P.; Geoffroy, S.; Prat, M. Three periods of drying of a single square capillary Tube. *Phys. Rev. Lett.* **2009**, *103*, 12.
(36) Peysson, Y.; Fleury, M.; Blázquez-Pascual, V. Drying rate measurements in convection- and diffusion-driven conditions on a shaly sandstone using nuclear magnetic resonance. *Transp. Porous Media* **2011**, *90* (3), 1001−1016.
(37) Prange, M.; Song, Y. Q. Understanding NMR T(2) spectral uncertainty. *J. Magn. Reson.* **2010**, *204* (1), 118−23.